# Materials Behaviour Analysis of 3D Printed Brass-PLA Filament



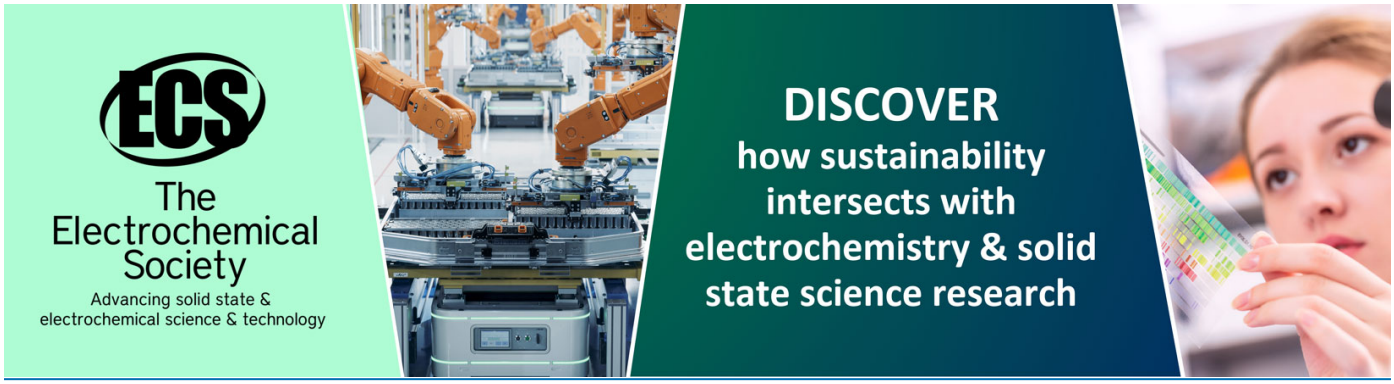

# Materials Behaviour Analysis of 3D Printed Brass-PLA Filament

**Dinesh Rajan[1], M. Samykano[1*], S. K. Suraparaju[2], K. Moorthy[3], K. Kadirgama[1], D. Ramasamy[1] & A. K. Pandey[4]**

[1]Faculty of Mechanical and Automotive Engineering Technology, Universiti Malaysia Pahang Al-Sultan Abdullah, 26600 Pekan, Pahang, Malaysia

[2]Centre for Research in Advanced Fluid and Process, University Malaysia Pahang Al-Sultan Abdullah, Lebuhraya Tun Razak, Gambang, Kuantan 26300, Pahang, Malaysia

[3]Faculty of Computer Systems & Software Engineering, Universiti Malaysia Pahang Al-Sultan Abdullah, Kuantan, Malaysia

[4]Research Centre for Nano-Materials and Energy Technology (RCNMET), School of Engineering and Technology, Sunway University, No. 5, Jalan Universiti, Bandar Sunway, Petaling Jaya 47500, Selangor Darul Ehsan, Malaysia

***Corresponding Author:** E-mail: mahendran@ump.edu.my (M. Samykano)

**Abstract**. The current study aims to bridge a crucial gap in existing research, potentially paving the way for a groundbreaking transformation in the development and application of PLA/Brass composites within diverse industries such as aerospace, automotive, consumer goods, and medical devices. The primary objective of this research is to assess the mechanical properties of a composite material made up of Polylactic Acid (PLA) and Brass, produced using Fused Deposition Modelling (FDM) 3D printing technology. Brass, renowned for its exceptional mechanical properties, has been integrated into PLA to form this composite material. The study employs various analytical techniques, including Fourier Transform Infrared Spectroscopy (FTIR), Scanning Electron Microscopy (SEM), and Energy-Dispersive X-ray Spectroscopy (EDX), to scrutinize the chemical and physical characteristics of the PLA/Brass composite. This research revolves around exploring the impact of different printing parameters on the mechanical behavior of the printed specimens. The investigation delves into aspects such as tensile strength, compression resistance, bending properties, and impact resistance. To achieve this, test specimens with varying compositions have been produced using a Raise3D N2 Plus FDM 3D printer, with careful manipulation of printing parameters such as layer height and printing speed. The compositional variations range from 15% wt. to 80% wt., with layer height values spanning 0.25 mm, 0.30 mm, and 0.35 mm, and printing speeds ranging from 20 mm/s to 40 mm/s. The outcomes of this research have revealed the distinct influences of specific printing parameters on various mechanical properties. For example, in the context of tensile testing, it was observed that the combination of a layer height of 0.25 mm and a printing speed of 30 mm/s resulted in the highest elastic modulus. Similarly, the study provides crucial insights into optimizing PLA/Brass composite material properties through controlled additive manufacturing parameters, catering to diverse application requirements. Key findings include an elastic modulus of 0.870 GPa, ultimate tensile strength of 17.53 MPa, yield strength (0.2% offset) of 15.47 MPa, bending strength of 42.25 MPa, bending modulus of 3.679 GPa, compression strength of 33.46 MPa, compression modulus of 5.748 GPa, and energy absorption of 0.246 J. This study advances our knowledge of PLA/brass composite while also providing a chance to create innovative materials.

## 1. Introduction

Additive manufacturing, commonly known as 3D printing, stands as a burgeoning field in component production. It involves the meticulous layer-by-layer construction of three-dimensional objects, enabling the fabrication of intricate geometries and optimized designs [1],[2]. Among the prevailing techniques in 3D printing, Fused Deposition Modelling (FDM) has gained widespread adoption. This process employs an indexing nozzle to deposit a thermoplastic material onto a platform. FDM offers distinct advantages including durability, user-friendliness, and streamlined manufacturing procedures [3].

In the realm of FDM, materials such as PLA (Polylactic Acid) and ABS (Acrylonitrile Butadiene Styrene) are frequently utilized due to their favorable thermal and rheological properties for component production [4]. Nonetheless, notable strides have been made in the development of new thermoplastic filaments for FDM, such as PLA/Copper, PLA/Steel, PLA/Brass, and PLA/Copper, which demonstrate enhanced thermal conductivity [5]. These materials find applications across diverse industries including automotive, electronics, biomedical, construction, aerospace, and appliances [6-10].

The judicious selection of printing parameters is pivotal in achieving optimal performance and mechanical integrity in FDM-manufactured products [5]. Variables like infill pattern, infill density, raster width, raster angle, layer thickness, printing speed, air gap, operating temperature, and build orientation wield significant influence over the mechanical properties of the printed specimen as well as the efficiency of the manufacturing process [4],[11],[12]. Several researchers have investigated the FDM process parameter's effect on mechanical behavior. Lanzotti et al.[13], found that increasing raster angle resulted in a drop in strength while lowering layer thickness increased tensile strength. According to Chacón et al.[1], specimens that had lesser layer thickness had greater tensile strength and ductility; these improved mechanical qualities were attained with flat edge orientation.

This study aims to comprehensively characterize the physical properties of PLA/Brass composites employing techniques such as Scanning Electron Microscopy (SEM), Energy Dispersive X-ray Spectroscopy (EDX), and Fourier Transform Infrared Spectroscopy (FTIR). Furthermore, it seeks to investigate the impact of different factors on the mechanical properties of PLA/Brass samples fabricated through FDM. Experimental tests, encompassing tensile, compression, and bending testing, will be conducted to ascertain the strength and stiffness of the printed samples [4], [5].

In summary, the project background, objectives, and scope are discussed in the introduction. The material and methods section describes the procedures and approaches used by the RAISE3D N2 Plus printer to carry out this study. Next, the design of the experiment consists of a list of the constant and variable parameters for setting up and calibrating the 3D printer. In the results and discussion, the characterization of the PLA/Brass's physical and chemical properties utilizing FTIR analysis and SEM + EDX analysis is included. Finally, the results and analysis of the mechanical testing which consists of tensile, compression, bending, and impact are then discussed.

## 2. Materials and Methods

During the experimental process, the tensile test specimens were created using the Idea Maker 3D Desktop Raise3D N2 Plus Printer with a 0.4 mm nozzle, and PLA filament with a 1.75 mm diameter was utilized. G-code files are generated through the Idea Maker slicing software that controls the printing process. Several factors, as indicated in Table 1, were maintained constant throughout the experiment to ensure precise and reliable results.

**Table 1.** Constant Printing Parameters.

| No | Parameters | Values (Kept Constant) |
|---|---|---|
| 1 | Horizontal Shell: solid layer | Top: 8 layers, Bottom: 7 layers |
| 2 | Fill Pattern | Concentric |
| 3 | Infill Percentage | 50% |
| 4 | Raster angle | 0° |
| 5 | Nozzle Speed | 0.4 mm |
| 6 | Filament Diameter | 1.75 mm |
| 7 | Extruder Temperature | 210°C |
| 8 | Bed Temperature | 60°C |

### *2.1. Design of Experiment*

The experiment's design includes the chosen parameters and their respective values for investigation. The three parameters selected are layer height, printing speed, and metal composition. Two weight percentages were chosen for metal composition: 15% and 80% of the metal. A concentric infill pattern and a 50% infill percentage were maintained throughout the experiment. In total, there were nine different combinations of parameters. Since there were two samples for each combination, a total of 18 specimens were printed. Additionally, these 18 specimens were multiplied by the two different Brass metal compositions, resulting in a total of 36 samples printed for each mechanical test. The list of parameter combinations is listed in Table 2.

**Table 2.** Parameter Combination List.

| Combination | Layer Height (mm) | Printing Speed(mm/s) |
|---|---|---|
| 1 | 0.25 | 20 |
| 2 | 0.25 | 30 |
| 3 | 0.25 | 40 |
| 4 | 0.30 | 20 |
| 5 | 0.30 | 30 |
| 6 | 0.30 | 40 |
| 7 | 0.35 | 20 |
| 8 | 0.35 | 30 |
| 9 | 0.35 | 40 |

### *2.2. Fabrication of 4 Types of Specimens*

The 3D model of the tensile, compression, bending, and impact geometries was created by using SOLIDWORKS 2021 edition. The tensile specimen’s dimension was determined based on the ASTM D638 type 1 standard. For the impact specimens, dimensions were defined according to the ASTM D256 standard. In contrast, the compression specimens were developed based on the ASTM D695 standard, and the bending specimens were based on the ASTM D690 standard. The design files were saved in .stl

format after the modeling process to be further processed using slicing software. In this project, Idea Maker was utilized as the slicing program.

The specimen's print settings, filament settings, and specific values for the printing parameters were adjusted following the experiment's design using the slicing software. The software then generates G-code instructions after slicing. The G-code files were then transferred to a Secure Digital (SD) card and inserted into the LCD of the 3D printer for recognition. During physical manufacturing, a PLA-Brass filament extruder with a heat block and integrated heating element was fed PLA-Brass filament. The filament was pushed into the heat block, where it melted with the assistance of gears and rollers inside the extruder. The molten material was then extruded through the nozzle of the heat block and deposited onto the printing platform layer by layer in the x and y axes using the movable FDM head [14]. The extruder head made the necessary adjustments and continued building layers until the complete physical replication of the CAD file was produced. The functioning mechanism of FDM is illustrated in Figure 1.

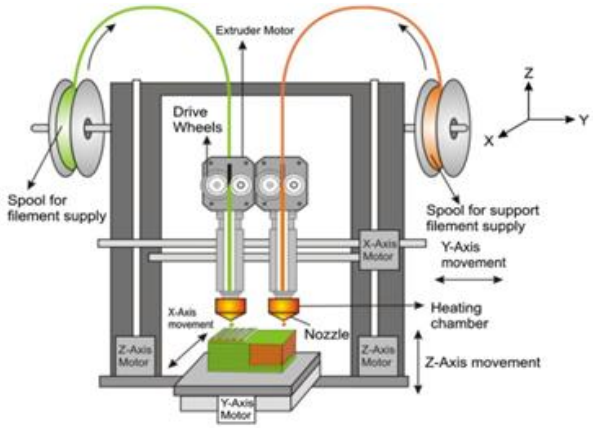


**Figure 1**. Working mechanism of FDM

### *2.3. Tensile Testing*

A tensile test was conducted using the INSTRON 3367 machine. This machine has a maximum load capacity of 50 kN. According to the ASTM D638 standard [15], the maximum testing rate allowed is 5 mm/min. Figure 2 illustrates the shape and dimensions of the Type 1 specimen used in the test, which has a thickness of 3.2 mm.

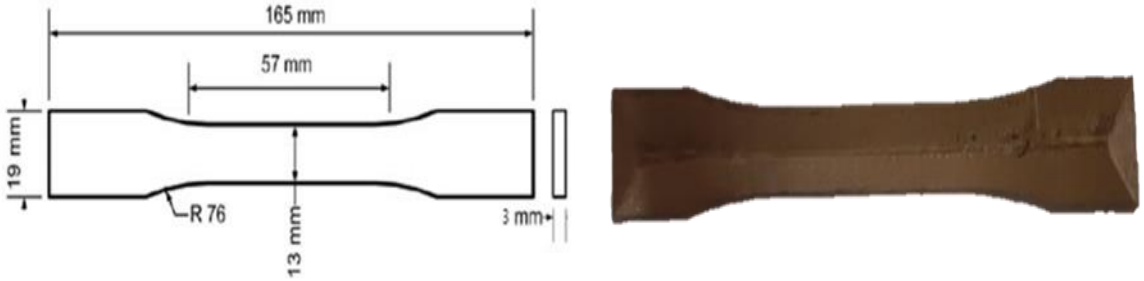


(a) (b)

**Figure 2.** (a) Type 1 specimen geometry according to ASTM D638 standard (b) A sample of printed tensile specimen

### *2.4. Compression Testing*

The compression test was performed using the INSTRON 3367 machine, which has a maximum load capacity of 50 kN. Next, the test was conducted following the ASTM Standard D695, which specifies a cylindrical specimen with a diameter of 12.7 mm and a length of 25.4 mm. The testing speed for compression is set at 1.3 ± 0.03 mm/min. Figure 3 provides a visual representation of the shape and dimensions of the compression specimen.

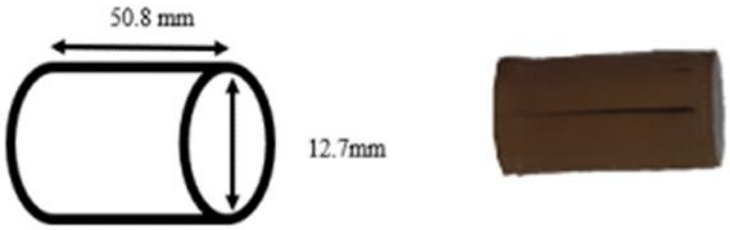


(a) (b)

**Figure 3.** (a) Specimen geometry and dimension according to ASTM D695 standard (b) A sample of printed compression specimen

### *2.5. Bending Test*

The bending properties of both metal weight compositions were evaluated using the INSTRON 3367 device, which has a maximum load capacity of 50 kN. The ASTM D790 standard was utilized for this test. The criterion for determining the specimen's cracking or deflection is when it exceeds 5% of its initial dimensions after the ASTM D790 test is completed. While various specimen shapes are acceptable, but most common ASTM specimen size is (3.2mm x 12.7mm x 125mm). Figure 4 illustrates the shape and dimensions of the bending specimen.

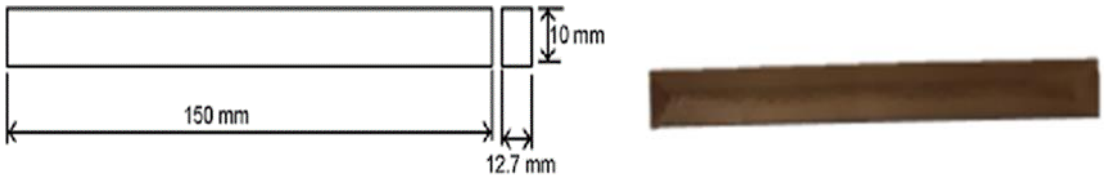


(a) (b)

**Figure 4.** (a) Specimen geometry and dimension according to ASTM D790 standard (b) A sample of printed bending specimen

### 2.6. *Impact Test*

The Izod impact test was selected as the testing method, following the ASTM D256 standard, for the printed samples. The dimensions of the test specimen will adhere to the requirements specified in ASTM D256, as outlined in Figure 5(a). The CEAST 9050 impact pendulum, which has an energy range of 0.5 to 50 J, will be used for the Izod impact test. Figure 5 provides a visual representation of the shape and dimensions of the impact specimen.

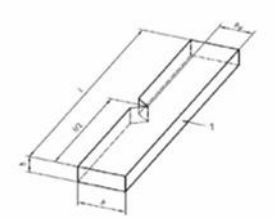

| ASTM standard | | |
|---|---|---|
| ASTM D256 | | Izod |
| Specimen dimensions | | |
| l = 63,5 mm | b = 12,7 mm | h = 6,35 or 3,17 mm |
| Notch dimensions | | |
| Angle = 45° | $b_n$ = 10,16 mm | radius = 0,25 mm (A) |

(a) (b)

**Figure 5.** (a) specimen's geometry and dimensions conform to the ASTM D256 standard (b) A sample of printed impact specimen

## 3. Results and Discussion

### *3.1. FTIR Analysis*

Fourier Transform Infrared (FTIR) analysis stands as a pivotal technique in the realms of materials science and chemistry. Its widespread application lies in dissecting the chemical composition of various materials. This method hinges on measuring the absorption of infrared light by the sample under scrutiny. When infrared light permeates the material, it engages with the different chemical bonds present, causing specific wavelengths to be absorbed. The resultant spectrum, a product of FTIR analysis, exhibits distinct peaks and troughs. Each of these points corresponds to the absorption and transmission of infrared light at precise wavelengths. These peaks and troughs are invaluable, offering profound insights into the functional groups and molecular structure inherent in the sample. Therefore, FTIR analysis emerges as an indispensable tool, enabling the identification and thorough analysis of a material's chemical composition.

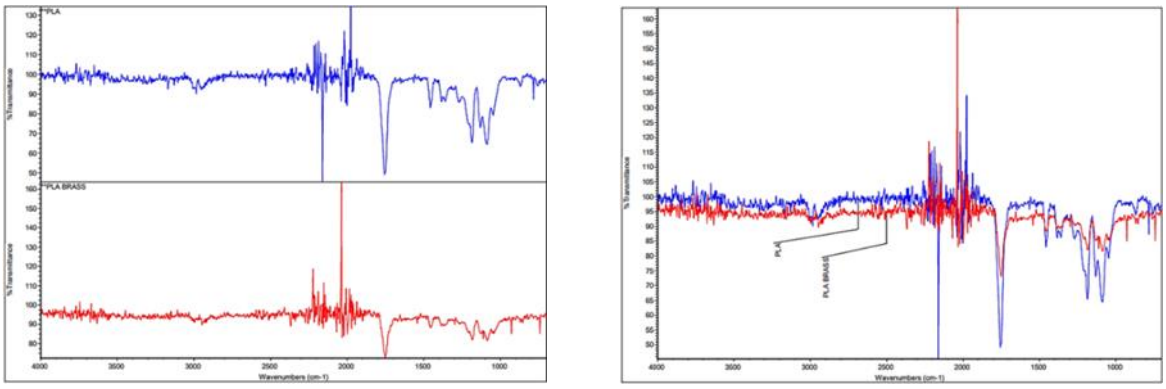

(a) (b)

**Figure 6.** (a) Analysis Stacking Graph for PLA and PLA/Brass (b) Analysis Overlay Graph for PLA and PLA/Brass

FTIR spectroscopy was utilized to examine the surface composition of materials used in the production of both Polylactic Acid (PLA) and PLA/Brass filament. In Figure 6(a), the obtained spectra are presented, revealing distinct characteristics associated with both PLA and PLA/Brass. These spectral features correspond to various functional groups, including carboxylic and carbonylic groups, as well as chemical bonds such as C–H, C=C, and C–O–C.

In the wavenumber range spanning from 2900 to 3200 $cm^{-1}$, discernible peaks linked to C–H compounds present in PLA are evident. Furthermore, the region encompassing 1086.27 to 1200 $cm^{-1}$ indicates the presence of oxygenated compounds. Notably, peaks at 1755.21 and 1455.58 $cm^{-1}$ signify the vibrational modes associated with carboxyl and/or carbonyl groups in PLA [16]. Intriguingly, these characteristic peaks from both PLA and PLA/Brass materials remain evident in the spectra, suggesting that the fingerprint region does not display significant distinctions. This observation can likely be attributed to the 15wt.% composition of metal within the PLA/Brass composite. Figure 6(b) presents an overlay graph, facilitating a direct comparison of the FTIR spectra between PLA and PLA/Brass, thus highlighting the remarkable similarities between these two materials.

### *3.2. SEM and EDX Analysis*

Scanning Electron Microscopy (SEM) and Energy-Dispersive X-ray Spectroscopy (EDX) stand as two complementary techniques extensively employed for the microscopic analysis of materials [17]. SEM facilitates the examination of a sample's surface topography with remarkable resolution by scanning it using an electron beam. This process generates signals that yield intricate images of the sample's surface, allowing researchers to scrutinize its morphology and structural characteristics. In conjunction with SEM, EDX is frequently utilized to dissect the elemental composition of materials. It achieves this by subjecting the sample to electron bombardment, which prompts the atoms within the material to emit distinctive X-rays. The ensuing energy spectrum of these emitted X-rays is subsequently analyzed. By delving into this energy spectrum, researchers can discern the elements present in the sample and glean insights into their relative abundance. SEM and EDX together provide invaluable insights into the composition, structure, and morphology of materials at a microscopic scale. Consequently, they empower researchers to explore and comprehend diverse material properties and phenomena

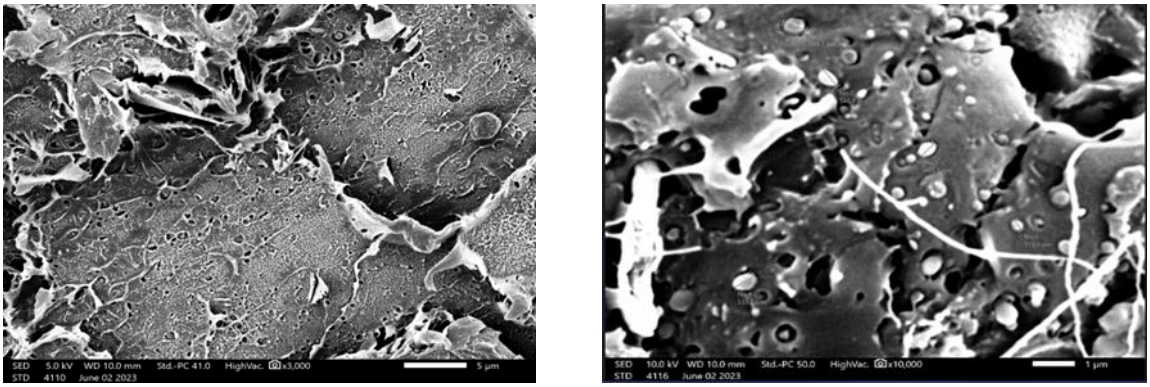

(a) (b)

**Figure 7.** (a) SEM micrograph of PLA/Brass without metal particle (b) SEM micrograph of PLA/Brass with metal particle

**Table 3.** Element content table of the PLA/Brass

| **Element** | **Line** | **Mass%** | **Atom%** |
|---|---|---|---|
| C | K | 48.50 ± 0.63 | 62.86 ± 0.82 |
| O | K | 33.73 ± 1.02 | 32.82 ± 1.00 |
| Cu | L | 13.32 ± 1.03 | 3.26 ± 0.25 |
| Zn | L | 4.45 ± 0.75 | 1.06 ± 0.18 |
| Total | | 100.00 | 100.00 |

Table 3 in this study presents the outcomes of SEM and EDX analyses carried out on a PLA/Brass filament that was manufactured under the Magma brand. This particular filament boasts a metal composition of 15wt.% and exhibits a diameter measuring 1.75mm. The meticulous analysis conducted has revealed the presence of minute metal particles embedded within the filament's structure. Upon a careful examination of the data provided in Figure 7(a), it becomes evident that the elemental composition of the filament is predominantly composed of carbon, comprising a significant portion of the mass, specifically 48.50%. In the given composition, oxygen stands out as the second most abundant element, making up a significant 33.73% of the total mass. Following closely is copper, contributing 13.32% of the mass, with zinc trailing behind at 4.45%. Figure 7(b) provides a detailed examination by zooming in, offering a closer inspection through a single-point analysis of the filament. This specific view unveils the dimensions of the metal particles within the filament, with their size measured in nanometers (nm).

### *3.3. Tensile Results*

The stress-strain curves were obtained through conducting tensile tests, serving as the foundation for the analysis of the mechanical properties of the material. In Figure 8, the stress-strain behavior of a particular specimen is depicted. This specimen was produced using printing parameters (0.30, 30) and accounts for 15% of the material composition.

Table 4 provides the average values of the yield strength, elastic modulus, and ultimate tensile strength for various sets of parameters. These values hold significant importance as they furnish valuable insights into how the printed specimens react when subjected to tension. They contribute to a comprehensive understanding of the mechanical characteristics exhibited by these printed materials.

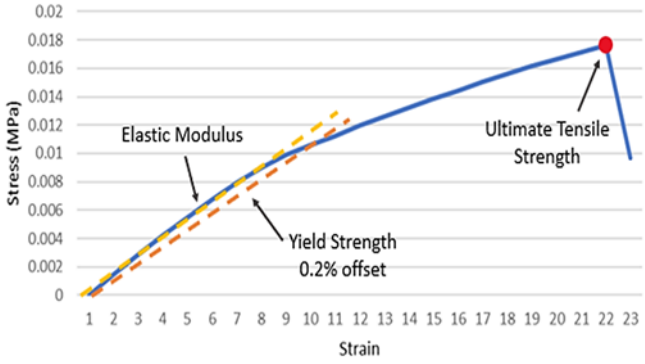


**Figure 8.** The stress-strain curve of a specific printing parameter (0.30, 30) – composition: 15 wt.%.

The stress-strain curve plays a pivotal role in understanding a material's mechanical properties. In this graphical representation, the x-axis represents the applied strain, indicating how much the material deforms. On the other hand, the y-axis shows the corresponding stress, which is the force experienced by the material per unit area. One crucial parameter extracted from this curve is the ultimate tensile strength (UTS). This value signifies the maximum stress a material can endure before undergoing significant plastic deformation. Essentially, it gauges the material's capacity to withstand tension without fracturing. Another vital aspect is the elastic modulus, often referred to as stiffness. This metric quantifies the material's resistance to deformation when subjected to applied stress. It is essentially represented by the slope of the linear segment of the stress-strain curve and serves as an indicator of the material's ability to revert to its original shape after the stress is relieved. The yield strength, on the other hand, delineates the stress necessary to induce a specific degree of plastic deformation in the material. This point on the curve marks the transition from the linear elastic phase to the plastic deformation phase, providing a pivotal insight into the material's behavior. These mechanical attributes hold

paramount importance in the prediction and understanding of material performance under diverse loading conditions. Consequently, they empower engineers and researchers in the judicious selection and design of materials tailored for specific applications.

**Table 4.** Average results of Elastic Modulus, Ultimate Tensile Strength and Yield Strength

| Layer Height, Printing Speed | Composition (%) | Elastic Modulus (GPa) | Ultimate Tensile Strength (MPa) | Yield Strength (MPa) |
|---|---|---|---|---|
| 0.25, 20 | 15 | 0.810 | 13.36 | 13.27 |
| 0.25, 30 | 15 | 0.870 | 16.08 | 13.55 |
| 0.25, 40 | 15 | 0.786 | 14.60 | 12.78 |
| 0.30, 20 | 15 | 0.810 | 17.11 | 13.42 |
| 0.30, 30 | 15 | 0.786 | 16.22 | 10.33 |
| 0.30, 40 | 15 | 0.792 | 14.94 | 12.92 |
| 0.35, 20 | 15 | 0.807 | 16.14 | 15.47 |
| 0.35, 30 | 15 | 0.820 | 17.53 | 14.41 |
| 0.35, 40 | 15 | 0.772 | 14.57 | 13.86 |
| 0.25, 20 | 80 | 0.620 | 11.14 | 8.43 |
| 0.25, 30 | 80 | 0.580 | 11.69 | 8.31 |
| 0.25, 40 | 80 | 0.620 | 11.78 | 8.52 |
| 0.30, 20 | 80 | 0.631 | 12.01 | 9.00 |
| 0.30, 30 | 80 | 0.622 | 11.62 | 8.40 |
| 0.30, 40 | 80 | 0.622 | 11.58 | 8.61 |
| 0.35, 20 | 80 | 0.657 | 12.15 | 8.88 |
| 0.35, 30 | 80 | 0.663 | 11.92 | 8.86 |
| 0.35, 40 | 80 | 0.657 | 12.31 | 9.01 |

Figures 9(a), 9(b), and 9(c) offer a visual representation of how parameter combinations (layer height, printing speed) and metal composition relate to mechanical properties such as ultimate tensile strength, elastic modulus, and yield strength. Figure 9(a) specifically depicts the influence of these combinations on ultimate tensile strength. By scrutinizing the graph, one can discern the impact of varying layer height, printing speed, and metal composition on the material's ultimate tensile strength. Moving forward to Figure 9(b), it clarifies the connection between different parameter combinations and the elastic modulus. This graph is instrumental in understanding how changes in layer height, printing speed, and metal composition impact the material's stiffness. Lastly, Figure 9(c) visually represents the relationship between various parameter combinations and yield strength. A careful analysis of this graph enables one to assess how different combinations of layer height, printing speed, and metal composition influence the material's ability to withstand plastic deformation. These graphical representations are invaluable tools for analyzing the impact of parameter combinations on the mechanical properties of the material. They assist in recognizing trends, correlations, or notable variations, ultimately enhancing the understanding and optimization of the manufacturing process and material selection for specific applications.

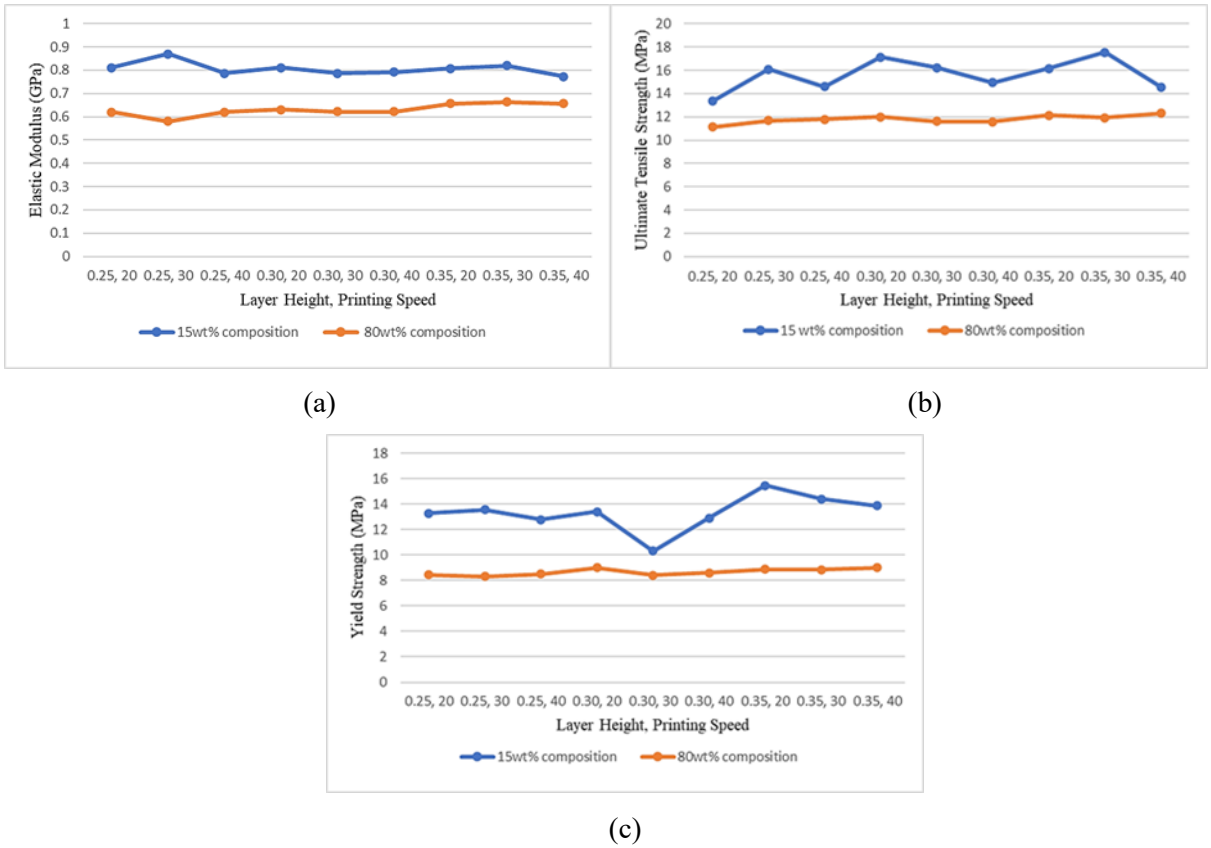


**Figure 9.** (a) Elastic Modulus against layer height and printing speed (b) Ultimate Tensile Strength against layer height and printing speed (c) Yield Strength against layer height and printing speed

The findings from the experiment, detailed in Table 4 and illustrated in Figures 9(a), 9(b), and 9(c), provide significant insights. Notably, specific combinations of layer height and printing speed stood out concerning the elastic modulus. For the 15wt.% composition, the most noteworthy results were obtained with settings (0.25,30), leading to a modulus of 0.870 GPa. Similarly, for the 80wt.% composition, the combination (0.35,30) yielded the highest modulus of 0.663 GPa. Conversely, combinations (0.35,40) and (0.25,30) produced the lowest elastic modulus values: 0.772 GPa for the 15wt.% composition and 0.52 GPa for the 80wt.% composition. Turning to ultimate tensile strength, the combination (0.35,30) emerged as the most effective, yielding a strength of 17.53 MPa for the 15wt.% composition. In contrast, the (0.25,20) combination resulted in the lowest values, with a strength of 13.36 MPa for the 15wt.% composition and 11.14 MPa for the 80wt.% composition.

Similarly, in terms of yield strength (0.2% offset), the combination (0.35,20) exhibited the highest values: 15.47 MPa for the 15wt.% composition. On the other hand, the combination (0.30,30) showed the lowest value: 10.33 MPa for the 15wt.% composition and 8.31 MPa for the 80wt.% composition at (0.25,30). Overall, the 15wt.% composition demonstrated higher elastic modulus, ultimate tensile strength, and yield strength (0.2% offset) than 80wt.% composition. These findings highlight the metal composition's influence on the printed specimens' mechanical properties. Additionally, the specific combinations of layer height and printing speed play a crucial role in achieving optimal mechanical performance. These insights are valuable for understanding the relationship between the printing parameters, metal composition, and mechanical properties. Previous studies have shown that adding fiber reinforcement increases the tensile strength of pure polymers, with findings for carbon fiber reaching 234 GPa [19], carbon nanotube reaching 270–950 GPa [20], pure PLA reaching 1280 MPa

[21], and pure ABS reaching at 1681.5 MPa [22]. They can guide future material selection and process optimization efforts for desired mechanical characteristics in 3D printing applications.

### *3.4. Compression Results*

Plastics with and without reinforcement can both have their compressive characteristics measured using the ASTM D695 test. Compression properties comprise two significant aspects: compressive strength and compressive modulus. Compressive strength denotes the capacity of a material to endure stress without breaking when subjected to a progressively increasing load. The strength is calculated by dividing the initial cross-sectional area of the compression specimen into the maximum load. Young's modulus of compression, often known as the compressive modulus, shares similarities with the tensile modulus and characterizes the material's rigidity when subjected to compressive forces. The calculation of the compression modulus relies on the magnitude of the applied compressive strength.

**Table 5.** Average results of Compression Strength and Compression Modulus

| Layer Height, Printing Speed | Composition (%) | Compression Strength (MPa) | Compression Modulus (GPa) |
|---|---|---|---|
| 0.25, 20 | 15 | 15.05 | 5.748 |
| 0.25, 30 | 15 | 23.62 | 4.154 |
| 0.25, 40 | 15 | 19.62 | 4.905 |
| 0.30, 20 | 15 | 26.69 | 3.628 |
| 0.30, 30 | 15 | 27.57 | 4.405 |
| 0.30, 40 | 15 | 28.58 | 3.277 |
| 0.35, 20 | 15 | 28.34 | 4.584 |
| 0.35, 30 | 15 | 33.46 | 3.427 |
| 0.35, 40 | 15 | 33.10 | 3.398 |
| 0.25, 20 | 80 | 6.35 | 2.648 |
| 0.25, 30 | 80 | 9.74 | 2.114 |
| 0.25, 40 | 80 | 10.3 | 2.430 |
| 0.30, 20 | 80 | 7.15 | 2.884 |
| 0.30, 30 | 80 | 10.3 | 2.535 |
| 0.30, 40 | 80 | 6.61 | 3.110 |
| 0.35, 20 | 80 | 9.36 | 2.443 |
| 0.35, 30 | 80 | 10.94 | 1.867 |
| 0.35, 40 | 80 | 12.00 | 1.653 |

The relationship between the independently collected mechanical property data and the combination of parameters was investigated, and the graphs were generated to identify any patterns or trends. Specifically, the impact of layer height, printing speed, and metal composition on compression strength and compression modulus was examined. The resulting graphs can be found in Figures 10: (a) and (b).

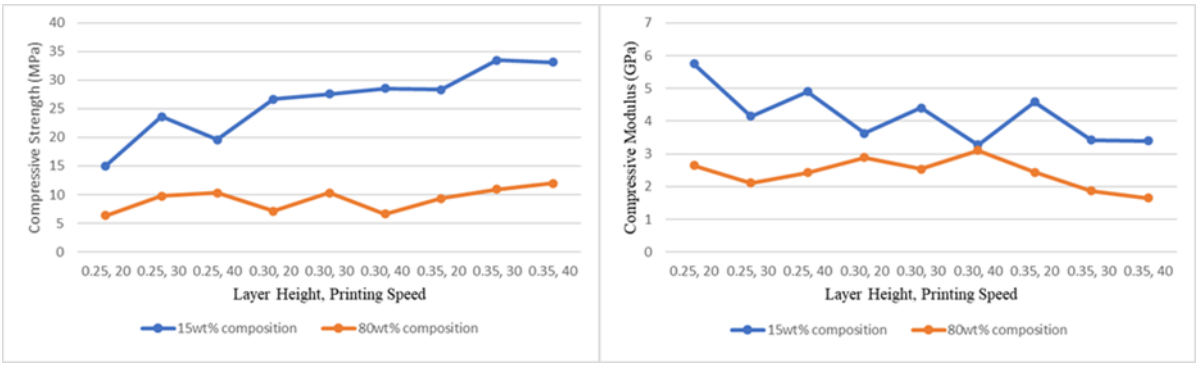


(a) (b)

**Figure 10.** (a) Compressive Strength against layer height and printing speed (b) Compressive Modulus against layer height and printing speed

The analysis of Table 5 and Figure 10(a) uncovers significant trends in compression strength concerning different combinations of layer height and printing speed, specifically focusing on two distinct material compositions, 15wt.% and 80wt.%. Notably, the highest compression strength was attained when employing a layer height and printing speed of (0.35, 30) for the 15wt.% composition, yielding an impressive strength value of 35.46MPa. In contrast, the combination (0.25, 20) exhibited the lowest compression strength for both compositions, with values of 15.05MPa for the 15wt.% composition and 6.35MPa for the 80wt.% composition. This indicates that (0.25, 20) is a suboptimal parameter set for compression strength, regardless of the material composition used. Upon comparing the two compositions, a clear pattern emerges - the 15wt.% material consistently demonstrated higher compression strength than the 80wt.% material.. This observation may have implications for the selection of material compositions in applications where compression strength is a critical factor. Turning attention to the analysis of compression modulus in Figure 10(b), it is apparent that the specimen with a layer height and printing speed of (0.25,20) in conjunction with a 15wt.% composition achieved the highest modulus at 5.748GPa. Conversely, the combination (0.30,40) displayed the lowest modulus for the 15wt.% composition, measuring at 3.277GPa. Furthermore, the combination (0.35,40) yielded the lowest modulus for the 80wt.% composition, measuring at 1.653GPa. Overall, the 15wt.% material demonstrated a higher compression modulus compared to the 80wt.% material. Low-infill specimens with cavities and voids are likely to significantly affect the strength of the specimen [18].

### *3.5. Bending Results*

The bending test results will primarily revolve around the analysis of bending properties, specifically bending strength and bending modulus. Bending strength pertains to a material's ability to withstand stress when subjected to bending forces perpendicular to its longitudinal axis, thereby indicating its stiffness [19]. On the other hand, bending modulus, also referred to as bending modulus, quantifies a material's resistance to bending. Following the completion of the bending test on the entire specimen, average values of the bending properties are calculated and organized into a tabular format. The relationship between the independently collected mechanical property data and the combination of parameters was investigated, and the graphs were generated to identify trends. Specifically, the impact of layer height, printing speed, and metal composition on bending strength and bending modulus was examined. The resulting graphs can be found in Figures 11: (a) and (b). These graphs visually represent how variations in the mentioned parameters and metal composition influence the bending strength and bending modulus.

**Table 6.** Average results of Compression Strength and Compression Modulus

| Layer Height, Printing Speed | Composition (%) | Bending Strength (MPa) | Bending Modulus (GPa) |
|---|---|---|---|
| 0.25, 20 | 15 | 33.08 | 2.483 |
| 0.25, 30 | 15 | 31.76 | 3.224 |
| 0.25, 40 | 15 | 31.97 | 3.075 |
| 0.30, 20 | 15 | 37.91 | 3.591 |
| 0.30, 30 | 15 | 42.25 | 3.679 |
| 0.30, 40 | 15 | 34.73 | 3.016 |
| 0.35, 20 | 15 | 35.49 | 3.050 |
| 0.35, 30 | 15 | 34.46 | 3.269 |
| 0.35, 40 | 15 | 37.38 | 3.315 |
| 0.25, 20 | 80 | 25.85 | 1.883 |
| 0.25, 30 | 80 | 25.71 | 1.897 |
| 0.25, 40 | 80 | 27.33 | 1.896 |
| 0.30, 20 | 80 | 18.81 | 1.736 |
| 0.30, 30 | 80 | 28.70 | 1.970 |
| 0.30, 40 | 80 | 16.98 | 2.118 |
| 0.35, 20 | 80 | 25.12 | 1.768 |
| 0.35, 30 | 80 | 26.34 | 1.915 |
| 0.35, 40 | 80 | 26.10 | 1.784 |

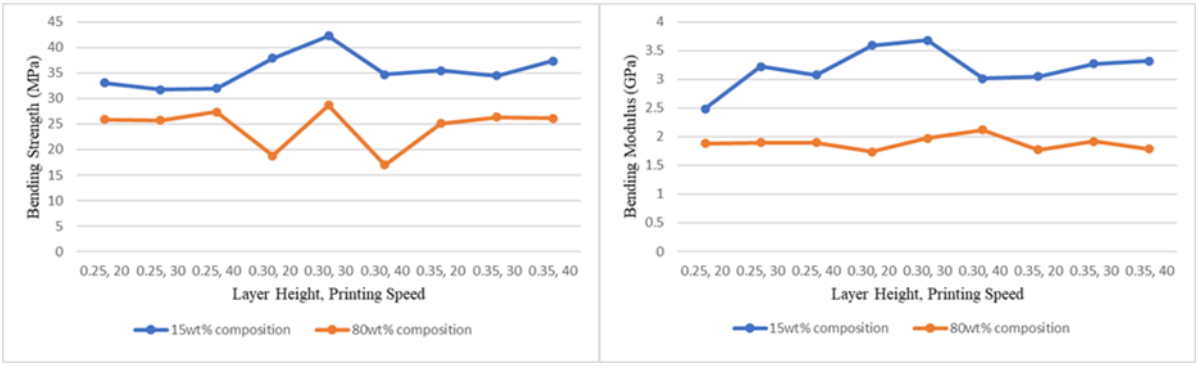


(a) (b)

**Figure 11.** (a) Bending Strength against layer height and printing speed (b) Bending Modulus against layer height and printing speed

Based on the data provided in Table 6 and Figure 11(a), it can be observed that the specimen with a 15wt.% composition, layer height, and printing speed of (0.30,30) demonstrated the highest bending strength at 42.25 MPa. On the other hand, the lowest bending strength for the 15wt.% composition was observed at (0.25,30) with a strength value of 31.76 MPa, for the specimens with an 80wt.% composition, the lowest bending strength was recorded at (0.30,40) with a strength of 16.98 MPa. Overall, the 15wt.% composition exhibited better bending strength compared to the 80wt.% composition. Similarly, based on Figure 11(b), it can be seen that the specimen with a 15wt.% composition, layer height, and printing speed of (0.30,30) displayed the highest bending modulus at 3.679GPa. Conversely, the lowest bending modulus for the 15wt.% composition was observed at (0.25,20) with a modulus value of 2.483GPa. For the specimens with an 80wt.% composition, the lowest bending modulus was recorded at (0.30,20) with a modulus of 1.736GPa.

### *3.6. Impact Results*

This test aims to measure the energy absorbed by the specimen. Energy absorbed refers to the amount of energy the specimen can withstand and dissipate during an impact test. This value provides insights into the material's toughness or hardness. The sample undergoes plastic deformation during the trial, particularly in the notch region. As the test progresses, the specimen absorbs energy and experiences work hardening within the plastic zone near the notch. Eventually, when the specimen reaches its energy absorption limit, a crack occurs, indicating the maximum energy it can absorb without fracturing.

**Table 7.** Average results of Energy Absorbed

| **Layer Height, Printing Speed** | **Composition (%)** | **Energy Absorbed** (J) |
|---|---|---|
| 0.25, 20 | 15 | 0.094 |
| 0.25, 30 | 15 | 0.108 |
| 0.25, 40 | 15 | 0.104 |
| 0.30, 20 | 15 | 0.102 |
| 0.30, 30 | 15 | 0.139 |
| 0.30, 40 | 15 | 0.122 |
| 0.35, 20 | 15 | 0.103 |
| 0.35, 30 | 15 | 0.111 |
| 0.35, 40 | 15 | 0.110 |
| 0.25, 20 | 80 | 0.193 |
| 0.25, 30 | 80 | 0.217 |
| 0.25, 40 | 80 | 0.249 |
| 0.30, 20 | 80 | 0.239 |
| 0.30, 30 | 80 | 0.246 |
| 0.30, 40 | 80 | 0.236 |
| 0.35, 20 | 80 | 0.220 |
| 0.35, 30 | 80 | 0.214 |
| 0.35, 40 | 80 | 0.209 |

The relationship between the independently collected mechanical property data and the combination of parameters was explored, and graphs were generated to identify the trends. Specifically, the impact of layer height, printing speed, and metal composition on energy absorbed and impact energy was examined. The resulting graphs can be found in Figure 12 (a). These graphs visually represent how variations in the mentioned parameters and metal composition influence the energy absorbed and impact energy.

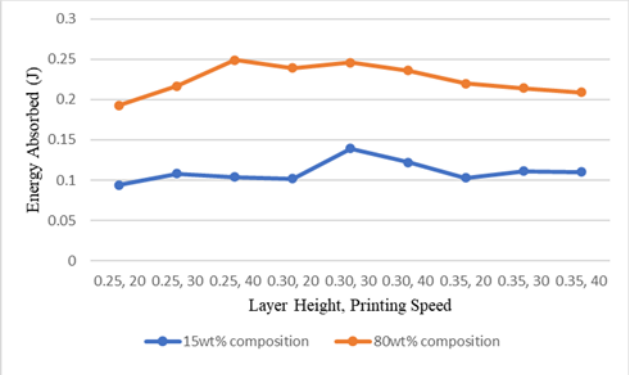


(a)

**Figure 12.** (a) Energy Absorbed against layer height and printing speed

Based on the data provided in Table 7 and Figure 12(a), it can be observed that the specimen with an 80wt.% composition, printed at a layer height and printing speed of (0.25,40), displayed the highest energy absorbed at 0.249 J. Conversely, the lowest energy absorbed was observed at (0.25,20) for both the 15wt.% and 80wt.% compositions, measuring 0.094 J and 0.193 J, respectively. The comparison between the two compositions, it can be concluded that the 80wt.% specimens absorbed more energy than the 15wt.% specimens.

## 4. Conclusion

In conclusion, this study focused on examining the physical and mechanical properties of PLA/Brass composites and analyzing the mechanical performance of 3D printed components made through fused deposition modeling. The study analyzed the impact of printing parameters (layer height, printing speed) and composition on various mechanical properties, including elastic modulus, ultimate tensile strength, yield strength, bending strength, bending modulus, compression strength, compression modulus, and energy absorbed. The results highlighted the significant influence of both printing parameters and composition on the mechanical properties of the PLA/Brass composites.

The specimens with a 15wt.% brass composition and specific printing parameter combinations exhibited the highest values for several mechanical properties. However, the optimum composition for impact properties was found to be 80wt.% Brass. The layer height and printing speed were found to have the most influence on the elastic modulus, while the composition had the greatest impact on the impact characteristics, we could conclude from the results above. These findings underscore the importance of selecting appropriate printing parameters and composition to optimize the mechanical characteristics of 3D printed PLA/Brass composites.

The research utilized the Raise3D N2 Plus Printer for conducting the experiments and reported on the maximum mechanical responses achieved within the investigated parameter ranges. In the future parameters such as infill pattern or raster angle also can be varied with the layer height and printing speed to identify the detailed effect of the printing parameters.

## Declaration of Competing Interest

In this paper, the authors declare that they do not have any known financial or personal relationships that might appear to have influenced the work.

## CRediT Authorship Contribution Statement

Dinesh Hasan Rajan: Conceptualization, Methodology, Writing-Original draft preparation. M. Samykano: Data curation, Investigation, Writing-Reviewing and Editing. K. Kadirgama: Visualization, Supervision, Validation, Writing- Reviewing and Editing. K. Moorthy: Visualization, Supervision, Validation, Writing- Reviewing and Editing. A. K. Pandey: Visualization, Supervision, Validation, Writing- Reviewing and Editing.

## Acknowledgements

The authors express their gratitude to Universiti Malaysia Pahang, Malaysia, for the financial support and resources provided through research grants RDU192218, which enabled the successful completion of this study.

## References

[1] J. M. Chacón, M. A. Caminero, E. García-Plaza, and P. J. Núñez, "Additive manufacturing of PLA structures using fused deposition modelling: Effect of process parameters on mechanical properties and their optimal selection," *Mater. Des.*, vol. 124, pp. 143–157, 2017, doi: 10.1016/j.matdes.2017.03.065.

[2] T. D. Ngo, A. Kashani, G. Imbalzano, K. T. Q. Nguyen, and D. Hui, "Additive manufacturing (3D printing): A review of materials, methods, applications and challenges," *Compos. Part B Eng.*, vol. 143, pp. 172–196, 2018, doi: 10.1016/j.compositesb.2018.02.012.

[3] V. Durga Prasada Rao, P. Rajiv, and V. Navya Geethika, "Effect of fused deposition modelling (FDM) process parameters on tensile strength of carbon fibre PLA," *Mater. Today Proc.*, vol. 18, no. xxxx, pp. 2012–2018, 2019, doi: 10.1016/j.matpr.2019.06.009.

[4] K. Rajan, M. Samykano, K. Kadirgama, W. S. W. Harun, and M. M. Rahman, *Fused deposition modeling: process, materials, parameters, properties, and applications*, vol. 120, no. 3–4. Springer London, 2022. doi: 10.1007/s00170-022-08860-7.

[5] T. Flaata, G. J. Michna, and T. Letcher, "Ht2017-4856," *Proc. ASME 2017 Heat Transf. Summer Conf.*, pp. 1–6, 2017.

[6] P. Parandoush and D. Lin, "A review on additive manufacturing of polymer-fiber composites," *Compos. Struct.*, vol. 182, pp. 36–53, 2017, doi: 10.1016/j.compstruct.2017.08.088.

[7] P. Guo, B. Zou, C. Huang, and H. Gao, "Study on microstructure, mechanical properties and machinability of efficiently additive manufactured AISI 316L stainless steel by high-power direct laser deposition," *J. Mater. Process. Technol.*, vol. 240, pp. 12–22, 2017, doi: 10.1016/j.jmatprotec.2016.09.005.

[8] H. Xing *et al.*, "Effect of particle size distribution on the preparation of ZTA ceramic paste applying for stereolithography 3D printing," *Powder Technol.*, vol. 359, pp. 314–322, 2020, doi: 10.1016/j.powtec.2019.09.066.

[9] H. Xing, B. Zou, X. Wang, Y. Hu, C. Huang, and K. Xue, "Fabrication and characterization of SiC whiskers toughened Al2O3 paste for stereolithography 3D printing applications," *J. Alloys Compd.*, vol. 828, p. 154347, 2020, doi: 10.1016/j.jallcom.2020.154347.

[10] X. Liu, B. Zou, H. Xing, and C. Huang, "The preparation of ZrO2-Al2O3 composite ceramic

by SLA-3D printing and sintering processing," *Ceram. Int.*, vol. 46, no. 1, pp. 937–944, 2020, doi: 10.1016/j.ceramint.2019.09.054.

[11] D. Popescu, A. Zapciu, C. Amza, F. Baciu, and R. Marinescu, "FDM process parameters influence over the mechanical properties of polymer specimens: A review," *Polym. Test.*, vol. 69, pp. 157–166, 2018, doi: 10.1016/j.polymertesting.2018.05.020.

[12] X. Liu, M. Zhang, S. Li, L. Si, J. Peng, and Y. Hu, "Mechanical property parametric appraisal of fused deposition modeling parts based on the gray Taguchi method," *Int. J. Adv. Manuf. Technol.*, vol. 89, no. 5–8, pp. 2387–2397, 2017, doi: 10.1007/s00170-016-9263-3.

[13] A. Lanzotti, M. Grasso, G. Staiano, and M. Martorelli, "The impact of process parameters on mechanical properties of parts fabricated in PLA with an open-source 3-D printer," *Rapid Prototyp. J.*, vol. 21, no. 5, pp. 604–617, 2015, doi: 10.1108/RPJ-09-2014-0135.

[14] O. S. Es-Said, J. Foyos, R. Noorani, M. Mendelson, R. Marloth, and B. A. Pregger, "Effect of layer orientation on mechanical properties of rapid prototyped samples," *Mater. Manuf. Process.*, vol. 15, no. 1, pp. 107–122, 2000, doi: 10.1080/10426910008912976.

[15] W. C. Smith and R. W. Dean, "Structural characteristics of fused deposition modeling polycarbonate material," *Polym. Test.*, vol. 32, no. 8, pp. 1306–1312, 2013, doi: 10.1016/j.polymertesting.2013.07.014.

[16] J. S. Stefano *et al.*, "New conductive filament ready-to-use for 3D-printing electrochemical (bio)sensors: Towards the detection of SARS-CoV-2," *Anal. Chim. Acta*, vol. 1191, 2022, doi: 10.1016/j.aca.2021.339372.

[17] C. Esposito Corcione, F. Gervaso, F. Scalera, F. Montagna, A. Sannino, and A. Maffezzoli, "The feasibility of printing polylactic acid–nanohydroxyapatite composites using a low-cost fused deposition modeling 3D printer," *J. Appl. Polym. Sci.*, vol. 134, no. 13, pp. 1–10, 2017, doi: 10.1002/app.44656.

[18] pp. 10597 subeshan, b., et al., 2018. investigating compression strengths of 3d printed polymeric infill specimens of various geometries. in: nano-, bio-, info-tech sensors, and 3d systems ii, international society for optics and photonics, "No Title".

[19] R. Maguteeswaran, P. Prathap, S. Satheeshkumar, and S. Madhu, "Effect of alkali treatment on novel natural fiber extracted from the stem of Lankaran acacia for polymer composite applications," *Biomass Convers. Biorefinery*, 2023, doi: 10.1007/s13399-023-04189-7.